

This document is confidential and is proprietary to the American Chemical Society and its authors. Do not copy or disclose without written permission. If you have received this item in error, notify the sender and delete all copies.

Highly conductive silver nanoparticles functionalized aramid fiber paper for electric heaters with rapid response and chemical stability

Journal:	<i>Industrial & Engineering Chemistry Research</i>
Manuscript ID	ie-2020-04005c.R2
Manuscript Type:	Article
Date Submitted by the Author:	25-Sep-2020
Complete List of Authors:	Zhou, Yanfen; Qingdao University, Sun, Zhenhua; Qingdao University, Jiang, Liang; Qingdao University, Chen, Shaojuan; Qingdao University Ma, Jianwei; Qingdao University, Zhou, Fenglei; University College London

SCHOLARONE™
Manuscripts

1
2
3
4
5
6
7
8
9
10
11
12
13
14
15
16
17
18
19
20
21
22
23
24
25
26
27
28
29
30
31
32
33
34
35
36
37
38
39
40
41
42
43
44
45
46
47
48
49
50
51
52
53
54
55
56
57
58
59
60

Highly conductive silver nanoparticles functionalized aramid fiber paper for electric heaters with rapid response and chemical stability

Yanfen Zhou^{†, ‡, §}, Zhenhua Sun[†], Liang Jiang^{†, *}, Shaojuan Chen^{†, †}, Jianwei Ma^{†, ‡, *}, Fenglei Zhou^{†, §}

[†]College of Textiles and Clothing, Qingdao University, Qingdao, 266071, P. R. China

[‡]Industrial Research Institute of Nonwovens and Technical Textiles, Qingdao, 266071, P. R. China

[†]Eco-Textile Collaborative Innovation Center, Qingdao University, Qingdao, 266071, P. R. China

[§]Centre for Medical Image Computing, University College London, London, WC1V 6LJ, UK

* Corresponding authors. Email: liang.jiang@qdu.edu.cn (L. Jiang), mjwfz@qdu.edu.cn (J. Ma).

Abstract: Electrical heaters with rapid response, robust mechanical properties and reliable chemical stability are highly desirable to meet the requirements for the development of high performance heating systems that can be used in extreme conditions. Herein, highly conductive silver nanoparticles (AgNPs) functionalized aramid fiber paper (AFP) based electrical heaters were fabricated through an efficient plasma treatment and electroless plating method. The AFP/AgNPs shows an outstanding electrical conductivity with the electrical resistance as low as 0.047 Ω /sq and maintains high electrical conductivity after 20 washing cycles and 1000 bending cycles. The AFP/AgNPs based electrical heater could reach a temperature of about 210 $^{\circ}$ C at a low voltage of 1 V with a rapid response time of 20 s. The electric heater also exhibited sufficient heating reliability, stability, and repeatability during long-term (up to 10000 s) and 180 repeated heating and cooling cycles. Moreover, the electrical heaters maintain satisfying heating performances even after being treated with acid/alkali solutions and various organic solvents. The overall performance of AFP/AgNPs based electrical heaters has been demonstrated in the application of water heating and ice melting, indicating their great potential for high-performance heating systems that can be used in various harsh conditions.

Keywords: Aramid fiber paper; Silver nanoparticles; Plasma treatment; Electroless plating; Electrical heater.

1. Introduction

With the increasing demands for smart wearables, optoelectronics and temperature-preservation device, electrical heaters which have light weight, high strength, ultra-flexibility and rapid response have received widespread attentions¹⁻⁵. Electrical heaters which increase temperature by converting electrical energy into thermal energy can meet the requirements for different scenes such as smart clothing, defogging, ice melting and water heating⁶⁻⁹. Under the electrical voltage, the electrical current formed in the electrical heaters overcomes the resistance to generate Joule heat, which is in accordance with Joule's law as shown in the following

equation:

$$Q = I^2 R t = U^2 t / R \quad (1)$$

Where U is electrical voltage, R is electrical resistance and t is the heating time. According to Joule's law, a low electrical resistance is conducive to generating more Joule heat to reach the saturation temperature at a low supplied voltage, thereby achieving better heating performance^{9, 10}.

Traditionally, indium tin oxide (ITO) had been used extensively in various electrical heaters due to its good electrical conductivity and transparency^{11, 12}. However, ITO is carcinogenic (category 2B carcinogen), brittle and non-flexible, which greatly limits its applications, especially in smart clothing that is used in human bodies^{9, 13}. As an alternative, electrical heaters based on conductive polymer composites have attracted increasing concerns in recent years¹⁴⁻¹⁶. Various conductive components including carbon nanotubes (CNTs)¹⁷⁻²⁰, graphene²¹⁻²⁴, MXene²⁵⁻²⁷, metal nanoparticles/nanowires²⁸⁻³⁷ have been widely used in fabricating conductive polymer composites. Among various conductive components, silver has the highest conductivity ($1.65 \times 10^{-8} \Omega \cdot \text{m}$ of resistivity) and is preferred in fabricating conductive polymer composites for electrical heaters with high heating performances^{29-31, 35}.

Conductive polymer composites can be fabricated through two different methods, one of which is blending the conductive components with the polymer matrix^{24, 38-41} and the other is coating the conductive components on the surface of various polymer substrates^{20, 25, 42-46}. Electrical heaters based on blended conductive polymer composites had better long-term fastness^{19, 21}, whereas in contrast, electrical heaters prepared with surface functionalized polymers showed faster thermal response time due to the heat generated by and dissipated on the surface^{5, 18, 26}, which achieved a balance between heat generation and heat dissipation rapidly.

Although there have been some progress on preparation of electrical heaters based on conductive polymer composites, it remains a challenge for electrical heaters to simultaneously

1
2
3 achieve high temperature at low voltage, rapid response and high stability in extreme conditions.
4
5 Aramid fiber paper (AFP), which is made by hot-press of high-performance pulp and short fiber,
6
7 could act as an excellent substrate for fabricating high-performance paper-based electrical
8
9 heaters owing to the advantages of high-strength, high-flexibility, high temperature resistance
10
11 and excellent chemical stability ⁴⁷.
12
13

14
15 In the present study, we proposed a method for preparing a highly conductive silver
16
17 nanoparticles (AgNPs) functionalized AFP (AFP/AgNPs) based electrical heater with rapid-
18
19 response and excellent chemical stability by combining low-temperature oxygen plasma
20
21 treatment and electroless plating. The plasma treatment significantly enhances the interfacial
22
23 interaction between the AFP substrate and the AgNPs, as well as the mechanical performance
24
25 of the AgNPs functionalized AFP through the etching effect and the introduction of oxygen-
26
27 containing groups. The electrical conductivity and heating performance of the AFP/AgNPs
28
29 were investigated. The results show that the AFP/AgNPs has an outstanding electrical
30
31 conductivity with the electrical resistance as low as 0.047 Ω/sq . The AFP/AgNPs based
32
33 electrical heaters exhibit rapid response, excellent stability and reliability upon long-term and
34
35 repeated heating/cooling cycles as well as satisfying heating performances after being subjected
36
37 to washing, bending deformation and chemical corrosion. The performance of the AFP/AgNPs
38
39 composites based heater were demonstrated in water heating and deicing.
40
41
42
43

44 **2. Experimental**

45 *2.1. Materials*

46
47 Meta-aramid fiber papers with a thickness of 0.18 mm were supplied by ZhongFang Special
48
49 Fiber Co., Ltd, Dongying, China. Ethanol, silver nitrate (AgNO_3), sodium hydroxide (NaOH),
50
51 ammonia ($\text{NH}_3 \cdot \text{H}_2\text{O}$), glucose, sodium hydroxide (NaOH), hydrochloric acid (HCl), acetone,
52
53 N-heptane and xylene were purchased from Sinopharm Chemical Reagent Co., Ltd, Shanghai,
54
55
56
57
58
59
60
China.

2.2. Preparation of AFP/AgNPs Composites

Initially, AFP were ultrasonically washed with 50 vol % of ethanol for 30 minutes to remove surface impurities and dried in vacuum at 60 °C for 2 h. Then, the AFP were treated by using a plasma treater (AS 400, Plasmatreat GmbH, Germany) at a nozzle speed of 1 m/min, a plasma cycle time of 80% and a nozzle height of 4-5 cm. Immediately after the plasma treatment, the AFP were immersed in a ammoniacal silver nitrate solution (5 ~ 30 g/L of AgNO₃ concentration) for 30 minutes and then, glucose (with a concentration of 30 g/L) as a reducing agent was added to the ammoniacal silver nitrate solution at a dropping rate of about 60 drops/minute. The reaction was allowed to proceed at 30 °C for 24 h. After electroless plating, the silver-coated MAFP was rinsed with deionized water three times and dried in vacuum oven at 60 °C for 24 hours. The AgNPs coated AFP obtained with AgNO₃ concentration of 5, 10, 15, 20 and 30 g/L was denoted as AFP/AgNPs-5, AFP/AgNPs-10, AFP/AgNPs-15, AFP/AgNPs-20, AFP/AgNPs-30, respectively.

2.3. Characterization

The surface morphology of AFP, plasma treated AFP and AFP/AgNPs was observed by using a scanning electron microscopy (SEM) (VEGA3, TESCAN, Czech). The surface element was scanned by using an energy dispersive spectrometer (EDS) (E1856-C2B, EDAX, USA). The chemical composition was investigated by using an X-ray photoelectron spectroscopy (XPS) (ESCALAB 250XI, Thermo Fisher Scientific, USA) with an Al K α X-ray source (1486.6 eV photons). The thermal property of AFP, plasma treated AFP and AFP/AgNPs composite papers was studied by using a TG/DSC synchronous thermal analyzer (STA 449 F3, NETZSCH GmbH, Germany). The measurement was conducted from 40 to 800 °C with a heating rate of 20 °C/min. The crystalline structure of the samples was investigated by using an X-ray diffractometer (XRD, Rigaku Ultima IV, Japan) of Cu K α radiation with a wavelength of 1.54056 Å. The mechanical property of different AFP was investigated by using a universal

1
2
3 tensile testing machine (Instron 5965, USA). The sheet resistance of AFP/AgNPs composite
4 papers was measured by using a multifunction digital four-probe tester (ST-2258C, Suzhou
5 Jingge Electronic Co., Ltd, China). For the heating performance tests, The AFP/AgNPs with a
6 dimension of 60 mm × 10 mm was mounted with conductive copper tape as the electrode. Silver
7 paste was employed to connect the tiny gap between samples and the copper tape to guarantee
8 good contact. Constant or repeatedly or gradiently changed voltages were applied to the
9 electrical heaters by using a precision power supply (B2901A, Keysight, USA). The real-time
10 surface temperature of the electrical heater was measured by using a contact thermometer
11 (UT320A, Uni-Trend Technology Co. Ltd, China) and the infrared thermal images were
12 captured by using an infrared thermal imager (TiS50, Fluke Electronic Instrumentation, USA).
13
14
15
16
17
18
19
20
21
22
23
24
25

26 **3. Results and discussion**

27 *3.1. Surface plasma treatment and silver plating of AFP*

28
29
30 Figure 1 illustrates the preparation process of AgNPs-coated AFP. Firstly, low temperature
31 plasma treatment was employed to activate the surface of AFP. In order to evaluate the effect
32 of plasma treatment, the surface morphology and chemical composition of AFP before and after
33 plasma treatment was studied. Figure 2a and b show the SEM image of pristine AFP and
34 plasma-treated AFP, respectively. It can be seen that different from pristine AFP (Figure 2a),
35 large amounts of etching spots (as noted by the red cycles) appeared on the plasma-treated AFP
36 surface (Figure 2b). EDS results (Figure S1, Supporting Information) further show that the
37 content of oxygen element increased from 23.88% to 28.73% after plasma treatment, indicating
38 more oxygen-containing groups in the surface of plasma-treated AFP.
39
40
41
42
43
44
45
46
47
48
49
50
51
52
53
54
55
56
57
58
59
60

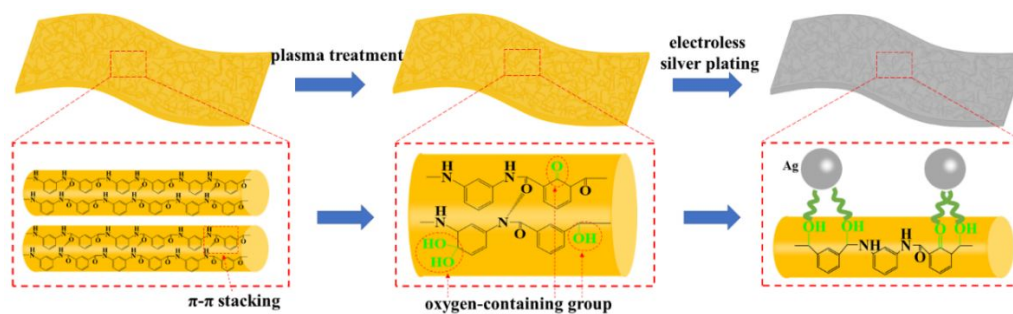


Figure 1. Schematic illustration for the fabrication of AgNPs functionalized AFP.

XPS was used to further study the effect of plasma treatment on the chemical composition of AFP. The XPS wide-scan spectra (Figure 2g) of pristine AFP and plasma-treated AFP showed three peaks at binding energy of about 285 eV, 400 eV and 532 eV corresponding to C 1s, N 1s and O 1s, respectively. The C 1s core-level spectrum of pristine AFP (Figure 2h) showed three peaks at binding energy of 284.4 eV for -C-C-/C-H, 285.4 eV for -C-N- and 287.9 eV for -C=O, which were ascribed to benzene ring and amide group in AFP. The C 1s core-level spectrum of plasma-treated AFP (Figure 2i) show two new peaks at binding energy of 286 eV and 288.9 eV belonging to -C-O- and -COO-, respectively, indicating that plasma treatment has introduced new oxygen-containing groups on the AFP surface. The N 1s core-level spectrum does not change after plasma treatment while the O 1s core-level spectrum of plasma-treated AFP show two new peaks at binding energy of 530 eV and 533 eV, which also confirms the introduction of oxygen-containing groups via plasma treatment (Figure S2, Supporting Information). Quantitative changes in chemical composition of the AFP before and after plasma treatment show that the content of carbon and nitrogen elements for AFP changed little after plasma treatment while the oxygen content varied obviously, with the O/C ratio increased from 0.14 to 0.97. The content of -C=O increased from 4.37% to 7.56% and the contents of new formed -C-O- and -COO- bonds were 2.64% and 3.22%, respectively. It is known that there is a strong π - π conjugation in the molecular chain of aramid, which hinders the reactivity of the group⁵. The introduction of those oxygen-containing groups after plasma treatment is beneficial to break π - π stacking balance and enhance the surface activity of AFP.

1
2
3 After electroless silver plating (the 2nd step in Figure 1), dense AgNPs deposited uniformly on
4 the AFP surface as can be observed from the SEM images (Figure 2c) and the EDS mapping
5 (Figure 2d) of AgNPs-coated AFP. The cross-sectional morphology (Figure 2e) shows that the
6 silver coating adhered tightly to the AFP surface. The strong signals derived from Ag in the
7 XPS wide-scan and Ag 3d core-level spectra of AFP/AgNPs in Figure 2g demonstrate that
8 AgNPs successfully deposited on the AFP surface. The Ag 3d core-level spectrum of
9 AFP/AgNPs composite paper show two peaks at binding energy of 374 eV for Ag 3d_{3/2} and
10 368 eV for Ag 3d_{5/2}, confirming that the silver particles were in the zerovalent state on the AFP
11 substrate surface. The formation of dense AgNPs on the plasma-treated MAFP surface is due
12 to the etching effect and the introduction of active oxygen-containing groups which could form
13 ionic and covalent interacting with AgNPs ⁴⁸. As shown in Figure 2f, the LED bulbs connected
14 in series and formed a logo of “QDU” that was lighted up when the AFP/AgNPs composite
15 paper was connected with a power supply of 220 V, indicating the high conductivity of the
16 AgNPs coated AFP.
17
18
19
20
21
22
23
24
25
26
27
28
29
30
31
32
33
34
35
36
37
38
39
40
41
42
43
44
45
46
47
48
49
50
51
52
53
54
55
56
57
58
59
60

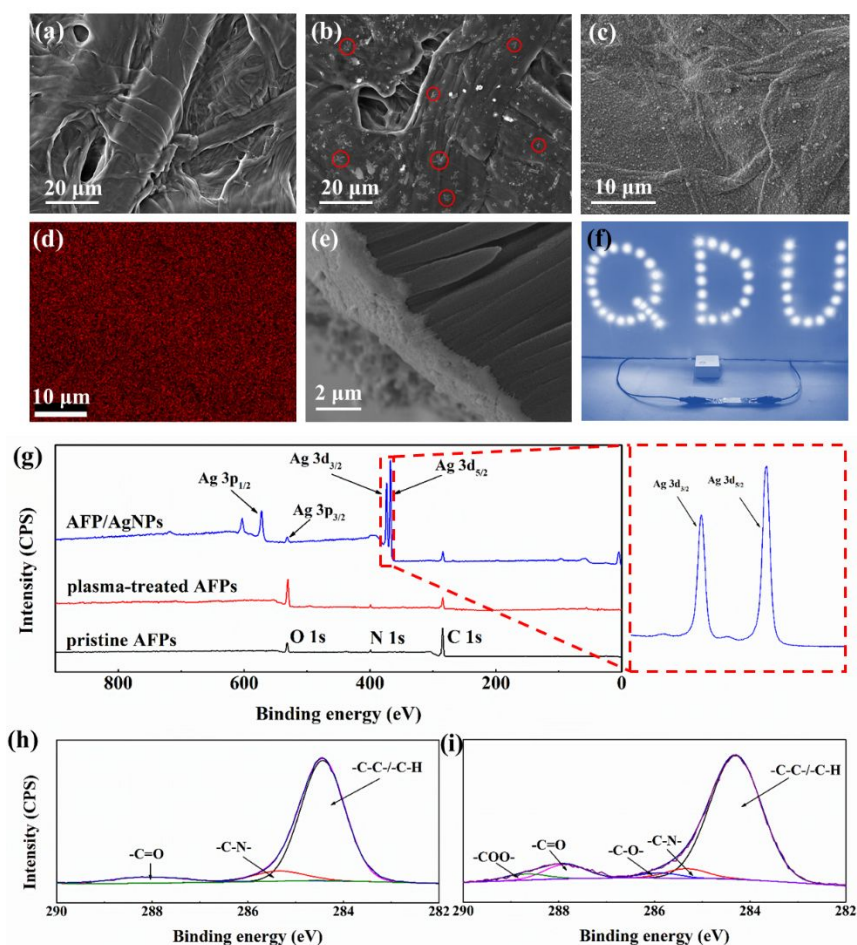


Figure 2. The SEM images of pristine AFP (a), plasma-treated AFP (the red cycles showing some of the etching pots) (b) and AgNPs-coated AFP (c); the EDS mapping of AgNPs-coated AFP (d); the cross-sectional morphology of AgNPs-coated AFP (e); lighting LED bulbs formed a logo of “QDU” when the AFP/AgNPs was connected with a power supply of 220 V (f); the XPS wide-scan spectra of pristine, plasma-treated and AgNPs-coated AFP (g); XPS spectra of C 1s peaks for pristine AFP (h) and plasma-treated AFP (i).

As a comparison, AgNPs-coated AFP which was not pre-treated with plasma was prepared, the SEM and EDS show that the AgNPs on the AFP surface was not continuous and no electrical conductivity was detected (Figure S3, Supporting Information).

3.2. XRD Analysis, Electrical, Thermal and Mechanical Properties of AFP/AgNPs

Figure 3a shows the XRD patterns of pristine AFP, plasma treated AFP and AgNPs coated AFP. The diffraction peak at the 2θ value of 27° , suggesting that the pristine AFP is a partly

1
2
3 crystalline ⁴⁹. The crystal structure of AFP did not change after plasma treatment, indicating
4 that the plasma treatment had no effect on the crystallinity of the AFP. Five new peaks at 2θ of
5 38.2°, 44.4°, 64.5°, 77.5°, 81.6° corresponding to the (1 1 1), (2 0 0), (2 2 0), (3 1 1) and (2 2
6 2) planes of face-centered cubic (FCC) lattice phase silver (JCPDS Card No.04-0783) appears
7 on AgNPs-coated AFP. SEM images and EDS mapping of AFP/AgNPs prepared with variable
8 AgNO₃ concentration ranging from 5 to 30 g/L show that the deposited silver layer for each
9 sample is uniform and the surface silver content increases from 84.40% to 95.88% (Figure S4,
10 Supporting Information). Figure 3b shows the TGA curves of pristine, plasma-treated and
11 AgNPs-coated AFP. It can be seen that the thermal degradation of all AFP samples is a two-
12 step stage process. The 1st stage in the temperature range of 40 °C to 200 °C was due to the
13 evaporation of bound water contained in the material and the 2nd stage starting from 430 °C was
14 attributed to partial dehydroxylation and alkoxide decomposition. These results indicate that
15 the thermal stability of AFP samples is good and is not apparently influenced by plasma
16 treatment and chemical deposition of AgNPs.

17
18
19
20
21
22
23
24
25
26
27
28
29
30
31
32
33
34
35
36
37
38
39
40
41
42
43
44
45
46
47
48
49
50
51
52
53
54
55
56
57
58
59
60

The relationship between AgNO₃ concentration and electrical sheet resistance (Figure 3c) shows that as the AgNO₃ concentration increases, the sheet resistance decreases sharply from 0.439 Ω/sq to about 0.076 Ω/sq when the AgNO₃ concentration increases from 5 to 15 g/L and then decreases slightly to 0.047 Ω/sq when the AgNO₃ concentration increase further to 30 g/L. The stability of AgNPs coating on AFP was evaluated by measuring the electrical conductivity after bending and washing. Figure 3d shows the change in sheet resistance of AFP/AgNPs-20 as an example with bending and washing cycles. It can be seen that the sheet resistance of AFP/AgNPs-20 increases from 0.049 Ω/sq to 0.11 Ω/sq after 1000 bending cycles and to 0.13 Ω/sq after 20 washing cycles. The above results suggest that the AFP/AgNPs have reliable bending and washing fastness.

Mechanical properties are of great importance considering the practical applications of AgNPs-

coated AFP. Figure 3e and 3f shows the typical stress-strain curves and the average tensile strength and elongation at break of pristine, plasma-treated and AgNPs-coated AFP, respectively. It can be seen that compared with pristine AFP, the tensile strength and elongation at break of plasma treated AFP increased by 16.1% and 115.4%, respectively. This was due to the fact that the increasing surface roughness and content of active oxygen-containing groups enhanced the bonding strength between adjacent fibers^{50, 51}. Interestingly, there are no obvious changes in both tensile strength and elongation at break between plasma treated AFP with and without AgNPs coating.

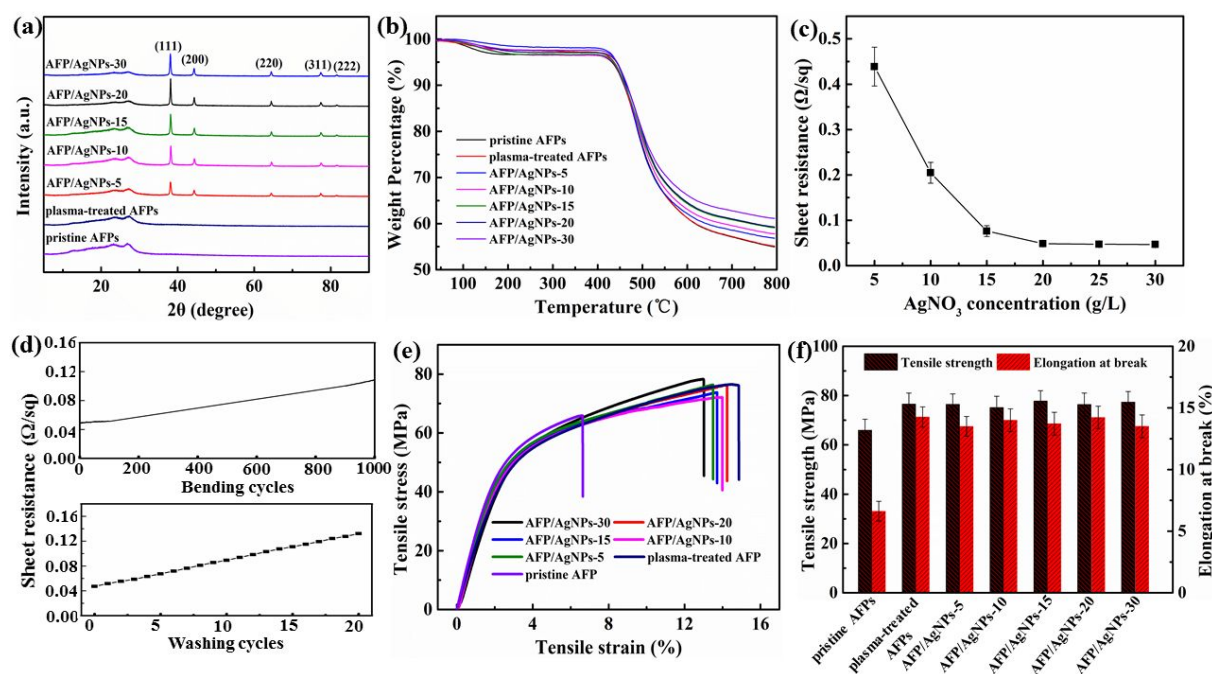


Figure 3. The XRD patterns of pristine AFP, plasma-treated AFP and AFP/AgNPs (a); the TGA curves of pristine AFP, plasma-treated AFP and AFP/AgNPs (b); the relationship between AgNO_3 concentration and sheet resistance (c); the variation of sheet resistance of AFP/AgNPs-20 with bending and washing cycles (d); the stress-strain curves (e) and the tensile strength and elongation at break (f) of pristine AFP, plasma-treated AFP and AFP/AgNPs.

3.3. Heating performance of AFP/AgNPs

Figure 4a and b shows the time-dependent temperature under different supplied voltages for the two electrical heaters based on AFP/AgNPs-5 and AgNPs-30, respectively. It can be seen that

1
2
3 for both electrical heaters, the saturation temperature (T_s) increases with increasing supplied
4 voltage and is reached within 20 s, demonstrating their rapid response; When the power was
5 switched off, the heater temperature decreases to room temperature within 25 s, demonstrating
6 equally rapid cooling response. At a supplied voltage of 1 V, the electrical heater base on
7 AFP/AgNPs-30 reached a saturation temperature of around 210 °C, which is higher than other
8 silver-coated polymer composites^{1-3, 52-54}.

9
10
11
12
13
14
15
16
17 Figure 4c shows the experimental data and the linear fittings of saturation temperature versus
18 applied voltage. When the voltage is supplied to the electrical heater, the electrical energy is
19 converted into thermal energy and the heater temperature rises rapidly; this process is
20 accompanied by the heat generation of the electrical heater and heat radiation to the surrounding
21 environment. According to the energy balance principle, the surface temperature of electrical
22 heaters would reach an equilibrium when the dissipated power by Joule heating is equal to the
23 power losses through conduction, convection, and radiation³⁴. Accordingly, the surface
24 temperature of electrical heaters could be calculated by using the following equation:

$$\frac{U^2}{R} = mc \frac{dT}{dt} + hA(T - T_0) \quad (2)$$

25
26
27
28
29
30
31
32
33
34
35
36
37
38
39
40
41
42
43
44
45
46
47
48
49
50
51
52
53
54
55
56
57
58
59
60
Where U is the supplied voltage, R is the electrical resistance of electrical heater, m is the mass
of the electrical heater, c is the specific heat capacity, h is the convective heat-transfer
coefficient, A is the area of electrical heater, T is the surface temperature and T_0 is the initial
ambient temperature. By integrating Eqn. 2 and taking $T(t=0) = T_0$, the time-dependent surface
temperature and T_s of electrical heaters could be obtained as shown below⁵:

$$T = T_0 + \frac{U^2}{RhA} (1 - e^{-(hA/mc)t}) \quad (3)$$

$$T_s = T_0 + \frac{U^2}{RhA} \quad (4)$$

It can be seen from Figure 4c that the saturation temperature of heaters shows an excellent linear
relationship with U^2 , suggesting that the saturation temperature achieved at various supplied

1
2
3 voltages can be accurately calculated by the linear fitting within the materials range.

4
5 Aramid fiber paper, as a high-performance substance, would also be thermally decomposed
6
7 from about 430 °C as indicated by the TGA measurement shown in Figure 3b. It can be seen
8
9 from Figure 4d that at a certain applied voltage, the heaters temperature reaches the highest and
10
11 then drops to zero, indicating the heater didn't function anymore. The applied voltage at which
12
13 the temperature starts to drop is 3.2 V and 2.1 V for AFP/AgNPs-5 and AFP/AgNPs-10 based
14
15 heater, respectively and about 1.8 V for AgNPs-15, AFP/AgNPs-20 and AFP/AgNPs-30 based
16
17 heaters. It can also be noted that the highest heating temperature at which all heaters stopped
18
19 function is around 430 °C, which is in consistent with the TGA results (Figure 3b).
20
21
22

23
24 Figure 4e shows the change in heating temperature upon the gradient voltages for AFP/AgNPs-
25
26 5 and AFP/AgNPs-30 based electrical heaters. It can be seen that as the voltage gradually
27
28 changes, the temperature of two heaters rapidly increases or decreases, suggesting the rapid and
29
30 controlled response of the heater to temperature by simply tuning the applied voltage. The
31
32 heating repeatability and long-term heating stability of AFP/AgNPs based electrical heater were
33
34 investigated by using AFP/AgNPs -30 as an example. It can be seen from Figure 4f that when
35
36 the electrical heater is subjected to an alternating voltage of 0 V and 1 V, the heater shows
37
38 simultaneous temperature change between room temperature (23.7 °C) and about 210 °C.
39
40 Moreover, there is no change in the heating/cooling behaviors of the heaters throughout the
41
42 repeated on/off voltage for 10000 s (180 cycles), demonstrating the excellent repeatability of
43
44 the electrical heaters. The stability of electrical heaters was also investigated by applying a
45
46 constant supplied voltage. It can be seen from Figure 4g that at a constant supplied voltage of
47
48 0.5 V, the T_s of the heaters based on AFP/AgNPs-30 is very stable at around 115 °C for the test
49
50 period of 10000 s, indicating good long-term stability of the heater.
51
52
53
54
55
56
57
58
59
60

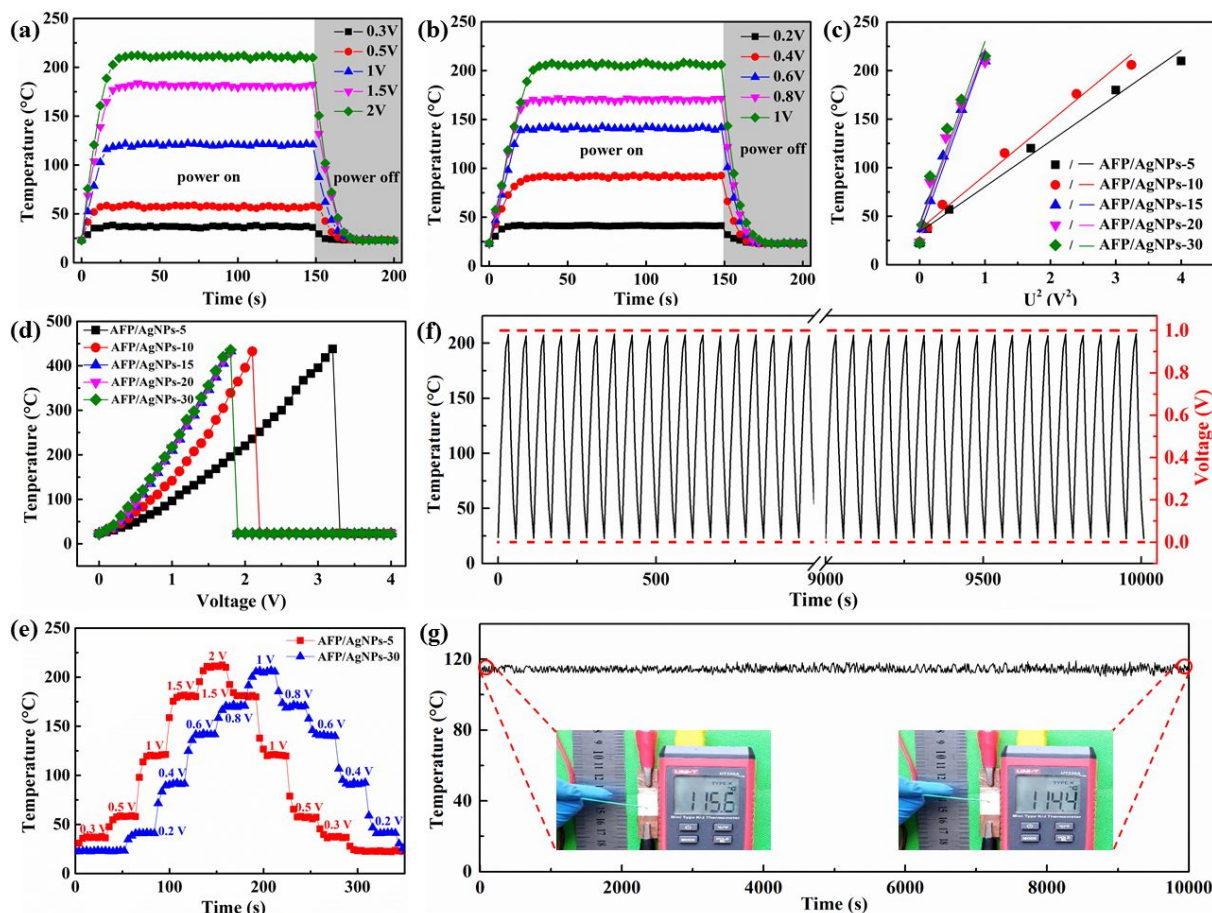


Figure 4. Time-dependent temperature at different supplied voltage for two electrical heaters based on AFP/AgNPs-5 (a) and AFP/AgNPs-30 (b); the linear fitting of saturation temperature versus U^2 (c); the relationship between surface temperature and voltage for AFP/AgNPs electrical heaters (d); surface temperature of electrical heaters based on AFP/AgNPs-5 and AFP/AgNPs-30 upon gradiently changed voltages (e); the heating repeatability upon alternating voltage of 0 V/1 V (f) and the long-term stability upon a supplied voltage of 0.5 V (g) for electrical heaters based on AFP/AgNPs-30.

Electrical heaters are inevitably subjected to various deformations and harsh environmental conditions during practical application. Therefore, it is important to evaluate the heating and cooling behaviors of the developed heaters in these conditions. Here the electrical heater prepared from AFP/AgNPs-15 was used as an example to demonstrate its stability in various extreme conditions.

Figure 5a-c show the heating performance of the electrical heaters before and after 1000

1
2
3 bending cycles or 20 washing cycles. It can be seen from Figure 5a that after bending or washing,
4 the saturation temperature of the electrical heater remains nearly unchanged, as revealed by the
5 fact all heaters reached around 100 °C within 20 s at a supplied voltage of 0.5 V. It can be seen
6 from Figure 5b-c that the electrical heater after 1000 bending cycles or 20 washing cycles still
7 demonstrates good stability at a constant voltage of 0.5 V. In addition, the electrical heaters
8 after bending or washing also show excellent repeatability under the alternating voltage of 0
9 V/1 V. The digital and infra-red (IR) images in Figure 5d show the performance of the flexible
10 electrical heaters based on AFP/AgNPs-15 in the “straight” and “bent” states with a supplied
11 voltage of 0.5 V. It can be seen that the electrical heater reaches 102.4 °C with a supplied
12 voltage of 0.5 V in straight state and the saturation temperature remains nearly unchanged in
13 the “bent” state (101.1 °C), indicating its feasibility to be used as a flexible electrical heater
14 candidate.

15
16
17 To evaluate the chemical stability of the AFP/AgNPs based electrical heater, the AFP/AgNPs-
18 15 were immersed in acid solution (pH = 2), neutral aqueous solution (pH = 7), alkali solution
19 (pH = 12) and various organic solvents including ethanol, acetone, N-heptane and xylene for 3
20 days, the electrical conductivity of AFP/AgNPs-15 and heating performance of the electrical
21 heaters based on the treated AFP/AgNPs-15 were evaluated. It can be seen from Figure 5e that
22 after being immersed in the above mentioned solutions and organic solvents for 3 days, the
23 sheet resistance of AFP/AgNPs-15 increased by 12.4%, 5.6%, 3.6%, 24.2%, 1.6%, 2.5% and
24 7.0%, respectively, and the saturation temperature of AFP/AgNPs-15 based electrical heater
25 decreased by 6.9%, 2.1%, 6.4%, 11.3%, 5.4%, 3.5% and 4.2%, respectively. It can be seen from
26 Figure 5f that the time-dependent temperature changes for electrical heaters prepared from
27 treated AFP/AgNPs-15 appear to be similar to that before immersion, and the response time is
28 still within 20 s. Figure S5 (Supporting Information) shows the repeatability with pulse voltage
29 of 0 V/1 V and long-term stability with constant voltage of 0.5 V for electrical heaters after
30
31
32
33
34
35
36
37
38
39
40
41
42
43
44
45
46
47
48
49
50
51
52
53
54
55
56
57
58
59
60

immersion. It can be seen that all electrical heaters with treated AFP/AgNPs-15 maintain excellent repeatability over hundreds of on/off voltage cycles and good long-term heating stability with a supplied voltage of 0.5 V for 10000 s. The above results demonstrate that the AFP/AgNPs based electrical heater has excellent chemical resistance. The corrosion resistance might be related with the enhanced surface roughness and hence the hydrophobicity of AFP/AgNPs (the water contact angle of AFP/AgNPs-15 is 106°), which to a certain degree, prevent the water or even the corrosion solution diffusing inside the material^{55,56}. Besides, the integrity of the silver coating layer is well preserved after immersion (Figure S6, Supporting Information) due to the enhanced interfacial interaction between AgNPs and AFP contributed by plasma treatment.

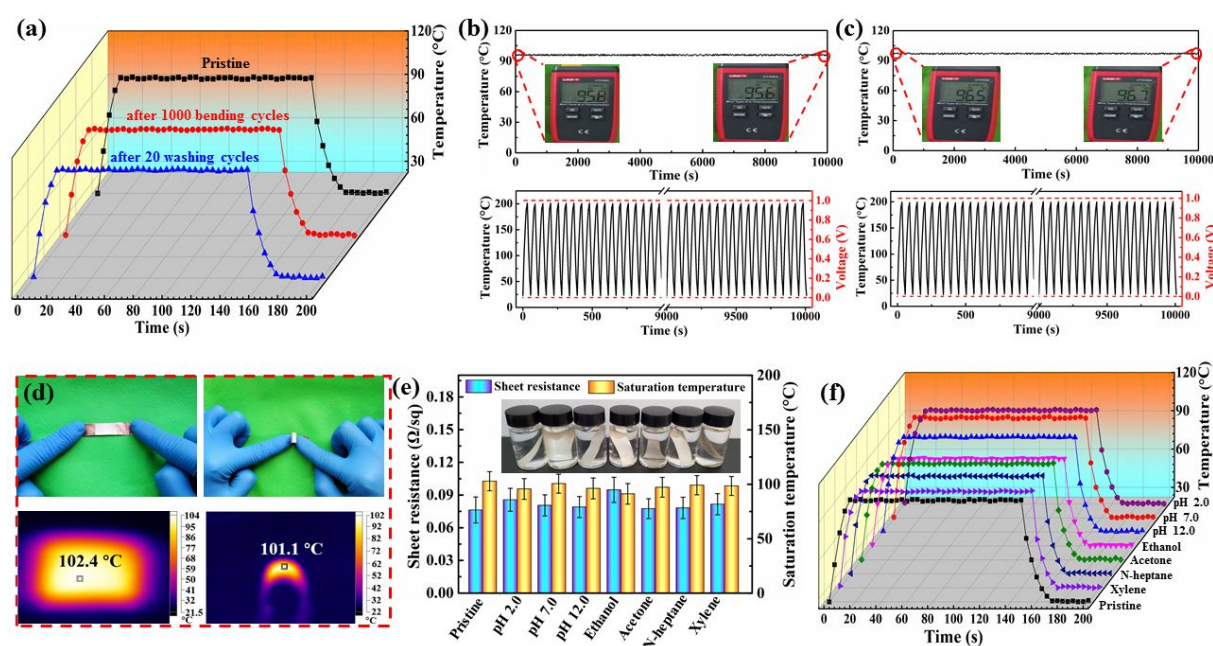
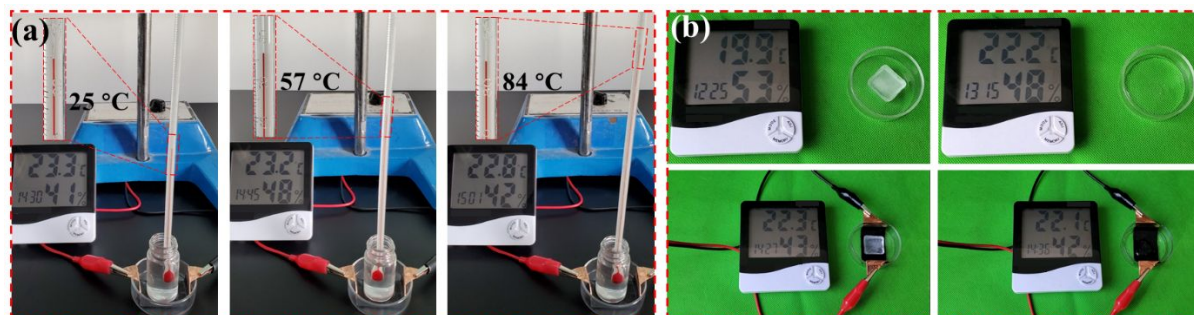


Figure 5. Time-dependent temperatures of electrical heaters based on AFP/AgNPs-15 after 1000 bending cycles and 20 washing cycles (a); the long-term stability and repeatability of electrical heaters after 1000 bending cycles (b) and 20 washing cycles (c); the digital and IR images of electrical heater in “straight” and “bent” state with supplied voltage of 0.5 V (d); the sheet resistance and saturation temperature of electrical heaters based on AFP/AgNPs-15 after soaking for 3 days (e) and time-dependent temperatures of electrical heaters after soaking for 3

1
2
3 days (f).
4

5 6 3.4. Applications of the AFP/AgNPs based electrical heater in water heating and ice melting

7
8 Figure 6a shows the use of an AFP/AgNPs-15 based heater to heat water. The electrical heater
9
10 sample with an area size of $2\text{ cm} \times 2\text{ cm}$ was placed at the bottom of a glass bottle containing
11
12 20 ml deionized water. The water was heated from $25\text{ }^\circ\text{C}$ to $57\text{ }^\circ\text{C}$ within 15 min upon the
13
14 supplied voltage of 1 V and then reached $84\text{ }^\circ\text{C}$ after another 15 min. Figure 6b shows the ice
15
16 melting by using AFP/AgNPs-15 based heater. When an ice cube with a weight of 10 grams
17
18 was left at room temperature without the heaters, it took as long as 50 min for the ice cube to
19
20 melt completely. Whereas in contrast, when an ice cube with the same weight was placed on
21
22 the top of the AFP/AgNPs-15 based heater with a size of $2\text{ cm} \times 2\text{ cm}$, the ice cube melt
23
24 completely in only 9 min at a supplied voltage of 0.5 V. The above results demonstrate that the
25
26 AFP/AgNPs based electrical heater has great potential for application in low-voltage and high-
27
28 efficiency water heating and ice melting.
29
30
31
32



44
45
46
47
48
49
50
51
52
53
54
55
56
57
58
59
60

Figure 6. The digital images of electrical heaters in water heating with a voltage of 1 V (a) and ice melting with a voltage of 0.5 V (b).

4. Conclusions

In conclusion, this work has reported the fabrication and performance of high-performance AgNPs functionalized AFP based electrical heaters through a very simple approach combining low-temperature oxygen plasma treatment and chemical deposition. The plasma treatment greatly favored the efficient deposition of AgNPs on the AFP surface through the etching effect and the introduction of oxygen-containing groups. The as-prepared AgNPs functionalized AFP

1
2
3 showed excellent electrical conductivity with the electrical resistance as low as 0.047 Ω/sq and
4
5 maintained high electrical conductivity after 20 washing cycles or 1000 bending cycles. The
6
7 electrical heater based on AFP/AgNPs reached a high temperature of about 210 $^{\circ}\text{C}$ at a low
8
9 voltage of 1 V and showed rapid response to the change in applied voltage. The electric heater
10
11 also possessed sufficient heating reliability, stability, and repeatability during long-term and
12
13 repeated heating and cooling cycles. In addition, the electrical heater exhibited outstanding heat
14
15 performance after being treated with acid/alkali solutions and various organic solvents. The
16
17 excellent heating performance of the AFP/AgNPs based electrical heater was demonstrated by
18
19 water heating and ice melting. It can be envisaged that the electrically conductive AFP is a
20
21 promising candidate for developing high performance flexible heating devices for applications
22
23 in extreme conditions.
24
25
26
27

28 **Acknowledgements**

29
30 The authors would like to thank the financial support from the Shandong Provincial Key
31
32 Research and Development Program, China (Grant no. 2019GGX102071, 2018GGX108003),
33
34 the National Key Research and Development Program of China (Grant no. 2017YFB0309805-
35
36 2), the Shandong “Taishan Youth Scholar Program” and the National Natural Science
37
38 Foundation of China (Grant no. 51703108).
39
40
41

42 **Appendix A. Supplementary data**

43
44 SEM images and EDS results of pristine AFP and plasma-treated AFP; the XPS N 1s and O 1s
45
46 spectra peaks for pristine AFP and plasma-treated AFP; the electrical resistance, SEM image
47
48 and EDS mapping of AgNPs-coated AFP without plasma treatment; the SEM image and EDS
49
50 mapping of silver-coated AFP obtained with different AgNO_3 concentration; heating
51
52 repeatability and long-term stability of AFP/AgNPs based electrical heater after being soaked
53
54 in acid/alkali solutions and various organic solvents; SEM image of AFP/AgNPs-15 after being
55
56 immersed in acid/alkali solutions and various organic solvents.
57
58
59
60

References

1. Hong, S.; Lee, H.; Lee, J.; Kwon, J.; Han, S.; Suh, Y. D.; Cho, H.; Shin, J.; Yeo, J.; Ko, S. H., Highly Stretchable and Transparent Metal Nanowire Heater for Wearable Electronics Applications. *Advanced Materials* **2015**, *27* (32), 4744-4751.
2. Jo, H. S.; Kwon, H. J.; Kim, T. G.; Park, C. W.; An, S.; Yarin, A. L.; Yoon, S. S., Wearable transparent thermal sensors and heaters based on metal-plated fibers and nanowires. *Nanoscale* **2018**, *10* (42), 19825-19834.
3. Lee, C. H.; Yun, Y. J.; Cho, H.; Lee, K. S.; Park, M.; Kim, H. Y.; Son, D. I., Environment-friendly, durable, electro-conductive, and highly transparent heaters based on silver nanowire functionalized keratin nanofiber textiles. *Journal of Materials Chemistry C* **2018**, *6* (29), 7847-7854.
4. Huang, Y.; Tian, Y.; Hang, C.; Liu, Y.; Wang, S.; Qi, M.; Zhang, H.; Zhao, J., Self-Limited Nanosoldering of Silver Nanowires for High-Performance Flexible Transparent Heaters. *ACS Applied Materials & Interfaces* **2019**, *11* (24), 21850-21858.
5. Ma, Z.; Kang, S.; Ma, J.; Shao, L.; Wei, A.; Liang, C.; Gu, J.; Yang, B.; Dong, D.; Wei, L.; Ji, Z., High-Performance and Rapid-Response Electrical Heaters Based on Ultraflexible, Heat-Resistant, and Mechanically Strong Aramid Nanofiber/Ag Nanowire Nanocomposite Papers. *ACS Nano* **2019**, *13* (7), 7578-7590.
6. Jang, N. S.; Kim, K. H.; Ha, S. H.; Jung, S. H.; Lee, H. M.; Kim, J. M., Simple Approach to High-Performance Stretchable Heaters Based on Kirigami Patterning of Conductive Paper for Wearable Thermotherapy Applications. *ACS Applied Materials & Interfaces* **2017**, *9* (23), 19612-19621.
7. Lordan, D.; Burke, M.; Manning, M.; Martin, A.; Amann, A.; O'Connell, D.; Murphy, R.; Lyons, C.; Quinn, A. J., Asymmetric Pentagonal Metal Meshes for Flexible Transparent Electrodes and Heaters. *ACS Applied Materials & Interfaces* **2017**, *9* (5), 4932-4940.
8. Bae, J. J.; Lim, S. C.; Han, G. H.; Jo, Y. W.; Doung, D. L.; Kim, E. S.; Chae, S. J.; Huy, T.

- 1
2
3 Q.; Van Luan, N.; Lee, Y. H., Heat Dissipation of Transparent Graphene Defoggers. *Advanced*
4 *Functional Materials* **2012**, *22* (22), 4819-4826.
- 5
6
7
8 9. Lee, J. G.; Lee, J. H.; An, S.; Kim, D. Y.; Kim, T. G.; Al-Deyab, S. S.; Yarin, A. L.; Yoon,
9 S. S., Highly flexible, stretchable, wearable, patternable and transparent heaters on complex 3D
10 surfaces formed from supersonically sprayed silver nanowires. *Journal of Materials Chemistry*
11 *A* **2017**, *5* (14), 6677-6685.
- 12
13
14
15 10. Li, P.; Ma, J.; Xu, H.; Xue, X.; Liu, Y., Highly stable copper wire/alumina/polyimide
16 composite films for stretchable and transparent heaters. *Journal of Materials Chemistry C* **2016**,
17 *4* (16), 3581-3591.
- 18
19
20
21 11. Gupta, R.; Kulkarni, G. U., Holistic Method for Evaluating Large Area Transparent
22 Conducting Electrodes. *ACS Applied Materials & Interfaces* **2013**, *5* (3), 730-736.
- 23
24
25
26 12. Xie, S.; Li, T.; Xu, Z.; Wang, Y.; Liu, X.; Guo, W., A high-response transparent heater
27 based on a CuS nanosheet film with superior mechanical flexibility and chemical stability.
28 *Nanoscale* **2018**, *10* (14), 6531-6538.
- 29
30
31
32 13. Kumar, A.; Zhou, C., The Race To Replace Tin-Doped Indium Oxide: Which Material
33 Will Win? *ACS Nano* **2010**, *4* (1), 11-14.
- 34
35
36
37 14. Sun, W. J.; Xu, L.; Jia, L. C.; Zhou, C. G.; Xiang, Y.; Yin, R. H.; Yan, D. X.; Tang, J. H.;
38 Li, Z. M., Highly conductive and stretchable carbon nanotube/thermoplastic polyurethane
39 composite for wearable heater. *Composites Science and Technology* **2019**, *181*, 107695.
- 40
41
42
43 15. Bustillos, J.; Zhang, C.; Boesl, B.; Agarwal, A., Three-Dimensional Graphene Foam–
44 Polymer Composite with Superior Deicing Efficiency and Strength. *ACS Applied Materials &*
45 *Interfaces* **2018**, *10* (5), 5022-5029.
- 46
47
48
49 16. Zhou, R.; Li, P.; Fan, Z.; Du, D.; Ouyang, J., Stretchable heaters with composites of an
50 intrinsically conductive polymer, reduced graphene oxide and an elastomer for wearable
51 thermotherapy. *Journal of Materials Chemistry C* **2017**, *5* (6), 1544-1551.
- 52
53
54
55
56
57
58
59
60

- 1
2
3 17. Zhan, Y. H.; Lago, E.; Santillo, C.; Castillo, A. E. D.; Hao, S.; Buonocore, G. G.; Chen, Z.
4
5 M.; Xia, H. S.; Lavorgna, M.; Bonaccorso, F., An anisotropic layer-by-layer carbon
6
7 nanotube/boron nitride/rubber composite and its application in electromagnetic shielding.
8
9 *Nanoscale* **2020**, *12* (14), 7782-7791.
10
11
12 18. Zhou, B.; Han, X.; Li, L.; Feng, Y.; Fang, T.; Zheng, G.; Wang, B.; Dai, K.; Liu, C.; Shen,
13
14 C., Ultrathin, flexible transparent Joule heater with fast response time based on single-walled
15
16 carbon nanotubes/poly(vinyl alcohol) film. *Composites Science and Technology* **2019**, *183*,
17
18 107796.
19
20
21 19. Ning, W.; Wang, Z.; Liu, P.; Zhou, D.; Yang, S.; Wang, J.; Li, Q.; Fan, S.; Jiang, K.,
22
23 Multifunctional super-aligned carbon nanotube/polyimide composite film heaters and actuators.
24
25 *Carbon* **2018**, *139*, 1136-1143.
26
27
28 20. Wang, Y.; Li, W.; Zhou, Y.; Jiang, L.; Ma, J.; Chen, S.; Jerrams, S.; Zhou, F., Fabrication
29
30 of high-performance wearable strain sensors by using CNTs-coated electrospun polyurethane
31
32 nanofibers. *J. Mater. Sci.* **2020**, *55* (26), 12592-12606.
33
34
35 21. Hazarika, A.; Deka, B. K.; Kim, D.; Jeong, H. E.; Park, Y. B.; Park, H. W., Woven Kevlar
36
37 Fiber/Polydimethylsiloxane/Reduced Graphene Oxide Composite-Based Personal Thermal
38
39 Management with Freestanding Cu–Ni Core–Shell Nanowires. *Nano Letters* **2018**, *18* (11),
40
41 6731-6739.
42
43
44 22. Zhang, Q.; Yu, Y.; Yang, K.; Zhang, B.; Zhao, K.; Xiong, G.; Zhang, X., Mechanically
45
46 robust and electrically conductive graphene-paper/glass-fibers/epoxy composites for stimuli-
47
48 responsive sensors and Joule heating heaters. *Carbon* **2017**, *124*, 296-307.
49
50
51 23. Liang, L. Y.; Xu, P. H.; Wang, Y. F.; Shang, Y.; Ma, J. M.; Su, F. M.; Feng, Y. Z.; He, C.
52
53 G.; Wang, Y. M.; Liu, C. T., Flexible polyvinylidene fluoride film with alternating oriented
54
55 graphene/Ni nanochains for electromagnetic interference shielding and thermal management.
56
57 *Chemical Engineering Journal* **2020**, *395*, 10.
58
59
60

- 1
2
3 24. Li, W.; Zhou, Y.; Wang, Y.; Li, Y.; Jiang, L.; Ma, J.; Chen, S., Highly Stretchable and
4 Sensitive SBS/Graphene Composite Fiber for Strain Sensors. *Macromolecular Materials and*
5
6 *Engineering* **2020**, *305* (3), 1900736.
7
8
9
10 25. Wang, Q. W.; Zhang, H. B.; Liu, J.; Zhao, S.; Xie, X.; Liu, L.; Yang, R.; Koratkar, N.; Yu,
11
12 Z. Z., Multifunctional and Water-Resistant MXene-Decorated Polyester Textiles with
13
14 Outstanding Electromagnetic Interference Shielding and Joule Heating Performances.
15
16 *Advanced Functional Materials* **2019**, *29* (7), 1806819.
17
18
19 26. Zhao, X.; Wang, L. Y.; Tang, C. Y.; Zha, X. J.; Liu, Y.; Su, B. H.; Ke, K.; Bao, R. Y.;
20
21 Yang, M. B.; Yang, W., Smart Ti₃C₂T_x MXene Fabric with Fast Humidity Response and Joule
22
23 Heating for Healthcare and Medical Therapy Applications. *ACS nano* **2020**, *14*, 8793-8805.
24
25
26 27. Li, L.; Cao, Y.; Liu, X.; Wang, J.; Yang, Y.; Wang, W., Multifunctional MXene-Based
27
28 Fireproof Electromagnetic Shielding Films with Exceptional Anisotropic Heat Dissipation
29
30 Capability and Joule Heating Performance. *ACS Applied Materials & Interfaces* **2020**, *12* (24),
31
32 27350-27360.
33
34
35 28. Zhou, Y.; Sun, Z.; Jiang, L.; Chen, S.; Ma, J.; Zhou, F., Flexible and conductive meta-
36
37 aramid fiber paper with high thermal and chemical stability for electromagnetic interference
38
39 shielding. *Applied Surface Science* **2020**, *533*, 147431.
40
41
42 29. Lan, W.; Chen, Y.; Yang, Z.; Han, W.; Zhou, J.; Zhang, Y.; Wang, J.; Tang, G.; Wei, Y.;
43
44 Dou, W.; Su, Q.; Xie, E., Ultraflexible Transparent Film Heater Made of Ag Nanowire/PVA
45
46 Composite for Rapid-Response Thermotherapy Pads. *ACS Applied Materials & Interfaces* **2017**,
47
48 *9* (7), 6644-6651.
49
50
51 30. Pyo, K. H.; Kim, J. W., Transparent and mechanically robust flexible heater based on
52
53 compositing of Ag nanowires and conductive polymer. *Composites Science and Technology*
54
55 **2016**, *133*, 7-14.
56
57
58 31. Wang, L.; Wang, D.; Wu, Z. F.; Luo, J. C.; Huang, X. W.; Gao, Q.; Lai, X. J.; Tang, L. C.;
59
60

1
2
3 Xue, H. G.; Gao, J. F., Self-Derived Superhydrophobic and Multifunctional Polymer Sponge
4 Composite with Excellent Joule Heating and Photothermal Performance for Strain/Pressure
5 Sensors. *Acs Applied Materials & Interfaces* **2020**, *12* (11), 13316-13326.
6
7

8
9
10 32. Liang, C.; Ruan, K.; Zhang, Y.; Gu, J., Multifunctional Flexible Electromagnetic
11 Interference Shielding Silver Nanowires/Cellulose Films with Excellent Thermal Management
12 and Joule Heating Performances. *ACS Applied Materials & Interfaces* **2020**, *12* (15), 18023-
13 18031.
14
15

16
17
18 33. Wu, L.; Wang, L.; Guo, Z.; Luo, J.; Xue, H.; Gao, J., Durable and Multifunctional
19 Superhydrophobic Coatings with Excellent Joule Heating and Electromagnetic Interference
20 Shielding Performance for Flexible Sensing Electronics. *ACS Applied Materials & Interfaces*
21 **2019**, *11* (37), 34338-34347.
22
23

24
25
26 34. Cheng, Y.; Zhang, H.; Wang, R.; Wang, X.; Zhai, H.; Wang, T.; Jin, Q.; Sun, J., Highly
27 Stretchable and Conductive Copper Nanowire Based Fibers with Hierarchical Structure for
28 Wearable Heaters. *ACS Applied Materials & Interfaces* **2016**, *8* (48), 32925-32933.
29
30

31
32
33 35. Wang, L.; Wang, D.; Wu, Z.; Luo, J.; Huang, X.; Gao, Q.; Lai, X.; Tang, L. C.; Xue, H.;
34 Gao, J., Self-Derived Superhydrophobic and Multifunctional Polymer Sponge Composite with
35 Excellent Joule Heating and Photothermal Performance for Strain/Pressure Sensors. *ACS*
36 *Applied Materials & Interfaces* **2020**, *12* (11), 13316-13326.
37
38

39
40
41 36. Sun, Z.; Zhou, Y.; Li, W.; Chen, S.; You, S.; Ma, J., Preparation of Silver-Plated Para-
42 Aramid Fiber by Employing Low-Temperature Oxygen Plasma Treatment and Dopamine
43 Functionalization. *Coatings* **2019**, *9* (10), 599.
44
45

46
47
48 37. Liu, C.; Liu, J.; Ning, X.; Chen, S.; Liu, Z.; Jiang, S.; Miao, D., The Effect of Polydopamine
49 on an Ag-Coated Polypropylene Nonwoven Fabric. *Polymers* **2019**, *11* (4), 627.
50
51

52
53
54 38. Shi, Y. D.; Li, J.; Tan, Y. J.; Chen, Y. F.; Wang, M., Percolation behavior of
55 electromagnetic interference shielding in polymer/multi-walled carbon nanotube
56
57
58
59
60

1
2
3 nanocomposites. *Composites Science and Technology* **2019**, *170*, 70-76.

4
5 39. Nallabothula, H.; Bhattacharjee, Y.; Samantara, L.; Bose, S., Processing-Mediated
6
7 Different States of Dispersion of Multiwalled Carbon Nanotubes in PDMS Nanocomposites
8
9 Influence EMI Shielding Performance. *ACS Omega* **2019**, *4* (1), 1781-1790.

10
11 40. Yang, X.; Fan, S.; Li, Y.; Guo, Y.; Li, Y.; Ruan, K.; Zhang, S.; Zhang, J.; Kong, J.; Gu, J.,
12
13 Synchronously improved electromagnetic interference shielding and thermal conductivity for
14
15 epoxy nanocomposites by constructing 3D copper nanowires/thermally annealed graphene
16
17 aerogel framework. *Composites Part A: Applied Science and Manufacturing* **2020**, *128*, 105670.

18
19 41. Wang, L.; Song, P.; Lin, C. T.; Kong, J.; Gu, J. W., 3D Shapeable, Superior Electrically
20
21 Conductive Cellulose Nanofibers/Ti₃C₂T_x MXene Aerogels/Epoxy Nanocomposites for
22
23 Promising EMI Shielding. *Research* **2020**, *2020*, 12.

24
25 42. Liu, L. X.; Chen, W.; Zhang, H. B.; Wang, Q. W.; Guan, F. L.; Yu, Z. Z., Flexible and
26
27 Multifunctional Silk Textiles with Biomimetic Leaf-Like MXene/Silver Nanowire
28
29 Nanostructures for Electromagnetic Interference Shielding, Humidity Monitoring, and Self-
30
31 Derived Hydrophobicity. *Advanced Functional Materials* **2019**, *29* (44), 1905197.

32
33 43. Jiang, L.; Zhou, Y.; Guo, Y.; Jiang, Z.; Chen, S.; Ma, J., Preparation of silver nanoparticle
34
35 functionalized polyamide fibers with antimicrobial activity and electrical conductivity. *Journal*
36
37 *of Applied Polymer Science* *136* (22), 47584.

38
39 44. Ma, Z.; Kang, S.; Ma, J.; Shao, L.; Zhang, Y.; Liu, C.; Wei, A.; Xiang, X.; Wei, L.; Gu, J.,
40
41 Ultraflexible and Mechanically Strong Double-Layered Aramid Nanofiber–Ti₃C₂T_x
42
43 MXene/Silver Nanowire Nanocomposite Papers for High-Performance Electromagnetic
44
45 Interference Shielding. *ACS Nano* **2020**, *14* (7), 8368-8382.

46
47 45. Luo, J.; Huo, L.; Wang, L.; Huang, X.; Li, J.; Guo, Z.; Gao, Q.; Hu, M.; Xue, H.; Gao, J.,
48
49 Superhydrophobic and multi-responsive fabric composite with excellent electro-photo-thermal
50
51 effect and electromagnetic interference shielding performance. *Chemical Engineering Journal*
52
53
54
55
56
57
58
59
60

1
2
3 **2020**, 391, 123537.

4
5 46. Zhang, X.; Jiang, S. X.; Cai, M.; Zhao, H. M.; Pan, F. K.; Miao, D. G.; Ning, X., Magnetron
6
7 sputtering deposition of Ag/Ag₂O bilayer films for highly efficient color generation on fabrics.

8
9
10 *Ceram. Int.* **2020**, 46 (9), 13342-13349.

11
12 47. Li, X.; Tang, C.; Wang, J.; Tian, W.; Hu, D., Analysis and mechanism of adsorption of
13
14 naphthenic mineral oil, water, formic acid, carbon dioxide, and methane on meta-aramid
15
16 insulation paper. *J. Mater. Sci.* **2019**, 54 (11), 8556-8570.

17
18 48. Zille, A.; Fernandes, M. M.; Francesko, A.; Tzanov, T.; Fernandes, M.; Oliveira, F. R.;
19
20 Almeida, L.; Amorim, T.; Carneiro, N.; Esteves, M. F.; Souto, A. P., Size and Aging Effects
21
22 on Antimicrobial Efficiency of Silver Nanoparticles Coated on Polyamide Fabrics Activated
23
24 by Atmospheric DBD Plasma. *ACS Applied Materials & Interfaces* **2015**, 7 (25), 13731-13744.

25
26 49. Wang, W.; Li, R.; Tian, M.; Liu, L.; Zou, H.; Zhao, X.; Zhang, L., Surface Silverized Meta-
27
28 Aramid Fibers Prepared by Bio-inspired Poly(dopamine) Functionalization. *ACS Applied*
29
30 *Materials & Interfaces* **2013**, 5 (6), 2062-2069.

31
32 50. Lu, Z.; Hu, W.; Xie, F.; Hao, Y.; Liu, G., Argon low-temperature plasma modification of
33
34 chopped aramid fiber and its effect on paper performance of aramid sheets. **2017**, 134 (34),
35
36 45215.

37
38 51. Hwang, Y. J.; Qiu, Y.; Zhang, C.; Jarrard, B.; Stedeford, R.; Tsai, J.; Park, Y. C.; McCord,
39
40 M., Effects of atmospheric pressure helium/air plasma treatment on adhesion and mechanical
41
42 properties of aramid fibers. *Journal of Adhesion Science and Technology* **2003**, 17 (6), 847-
43
44 860.

45
46 52. Choi, S.; Park, J.; Hyun, W.; Kim, J.; Kim, J.; Lee, Y. B.; Song, C.; Hwang, H. J.; Kim, J.
47
48 H.; Hyeon, T.; Kim, D.-H., Stretchable Heater Using Ligand-Exchanged Silver Nanowire
49
50 Nanocomposite for Wearable Articular Thermotherapy. *ACS Nano* **2015**, 9 (6), 6626-6633.

51
52 53. Hsu, P. C.; Liu, X.; Liu, C.; Xie, X.; Lee, H. R.; Welch, A. J.; Zhao, T.; Cui, Y., Personal
53
54
55
56
57
58
59
60

1
2
3 Thermal Management by Metallic Nanowire-Coated Textile. *Nano Letters* **2015**, *15* (1), 365-
4
5 371.

6
7
8 54. Kim, T.; Kim, Y. W.; Lee, H. S.; Kim, H.; Yang, W. S.; Suh, K. S., Uniformly
9
10 Interconnected Silver-Nanowire Networks for Transparent Film Heaters. **2013**, *23* (10), 1250-
11
12 1255.

13
14
15 55. Gao, J.; Luo, J.; Wang, L.; Huang, X.; Wang, H.; Song, X.; Hu, M.; Tang, L. C.; Xue, H.,
16
17 Flexible, superhydrophobic and highly conductive composite based on non-woven
18
19 polypropylene fabric for electromagnetic interference shielding. *Chemical Engineering Journal*
20
21 **2019**, *364*, 493-502.

22
23
24 56. Lin, L.; Wang, L.; Li, B.; Luo, J.; Huang, X.; Gao, Q.; Xue, H.; Gao, J., Dual conductive
25
26 network enabled superhydrophobic and high performance strain sensors with outstanding
27
28 electro-thermal performance and extremely high gauge factors. *Chemical Engineering Journal*
29
30 **2020**, *385*, 123391.

1
2
3
4
5
6
7
8
9
10
11
12
13
14
15
16
17
18
19
20
21
22
23
24
25
26
27
28
29
30
31
32
33
34
35
36
37
38
39
40
41
42
43
44
45
46
47
48
49
50
51
52
53
54
55
56
57
58
59
60

Table of Contents

AgNPs coated meta-aramid fiber paper

